Journal of Anatomy

J. Anat. (2014) doi: 10.1111/joa.12252

An investigation of matching symmetry in the human pinnae with possible implications for 3D ear recognition and sound localization

Peter Claes,[1] Jonas Reijniers,[2] Mark D. Shriver,[3] Jonatan Snyders,[1] Paul Suetens,[1] Joachim Nielandt,[4] Guy De Tré[4] and Dirk Vandermeulen[1]

[1]*Medical Image Computing, ESAT/PSI, Department of Electrical Engineering, KU Leuven, Medical Imaging Research Center, iMinds, Medical IT Department, UZ Leuven, Leuven, Belgium*
[2]*Department of Biology, University of Antwerp, Antwerp, Belgium*
[3]*Department of Anthropology, Pennsylvania State University, University Park, PA, USA*
[4]*Department of Telecommunications and Information Processing, Database, Document and Content Management Research Group, Ghent University, Ghent, Belgium*

Abstract

The human external ears, or pinnae, have an intriguing shape and, like most parts of the human external body, bilateral symmetry is observed between left and right. It is a well-known part of our auditory sensory system and mediates the spatial localization of incoming sounds in 3D from monaural cues due to its shape-specific filtering as well as binaural cues due to the paired bilateral locations of the left and right ears. Another less broadly appreciated aspect of the human pinna shape is its uniqueness from one individual to another, which is on the level of what is seen in fingerprints and facial features. This makes pinnae very useful in human identification, which is of great interest in biometrics and forensics. Anatomically, the type of symmetry observed is known as matching symmetry, with structures present as separate mirror copies on both sides of the body, and in this work we report the first such investigation of the human pinna in 3D. Within the framework of geometric morphometrics, we started by partitioning ear shape, represented in a spatially dense way, into patterns of symmetry and asymmetry, following a two-factor ANOVA design. Matching symmetry was measured in all substructures of the pinna anatomy. However, substructures that 'stick out' such as the helix, tragus, and lobule also contained a fair degree of asymmetry. In contrast, substructures such as the conchae, antitragus, and antihelix expressed relatively stronger degrees of symmetric variation in relation to their levels of asymmetry. Insights gained from this study were injected into an accompanying identification setup exploiting matching symmetry where improved performance is demonstrated. Finally, possible implications of the results in the context of ear recognition as well as sound localization are discussed.
Key words: ear recognition; geometric morphometrics; matching symmetry; sound localization; spatially dense.

Introduction

The human external ear, or pinna, is a well-known part of our auditory sensory system and exhibits bilateral symmetry like most parts of the external human body. The pinna's anatomy is relatively complex in comparison with the rest of the external human body, with highly curved and intertwined substructures (Fig. 1). Its shape, however, is far from arbitrary and has evolved to allow for spatial localization of sounds (Blauert, 1997). Complemented with the inter-aural time difference between both ears, which carries information on the horizontal position of the sound source, the acoustic (spectral) content of the binaural sound is filtered by the morphology of the head and ears in ways that allow the listener to further pinpoint the location of the sound source. Depending on the direction from where the sound originates, the body/head/ears filter away some frequencies, while reinforcing others, resulting in the so-called head-related transfer function (HRTF; Wightman & Kistler, 1989a): with a particular direction corresponding to a proper spectral filtering. Hence, analyzing the spectrum of the incoming sound, the observer can extract information on the direction from which the sounds originate. The

Correspondence
Peter Claes, Medical Image Computing, ESAT/PSI, Department of Electrical Engineering, KU Leuven, Medical Imaging Research Center, iMinds, Medical IT Department, UZ Leuven, Herestraat 49, Bus 7003, 3000 Leuven, Belgium. E: peter.claes@esat.kuleuven.be

Accepted for publication *24 September 2014*

external ear has evolved to operate best when subjected to sounds that humans are confronted with in their natural environment (broadband) and to be most sensitive and informative about directions that are most relevant to humans (Reijniers et al. 2014). Because of the limited physical dimensions of the outer ears, spatial cues introduced to the outer ears are mainly restricted to the high frequency part of the spectrum (above 4 kHz).

Another, less known, aspect of the human pinna shape is its uniqueness from one individual to another. This has been shown most exhaustively in work by Alfred Iannarelli, who compared more than 10 000 ears. In a subsequent study he also examined ears from fraternal as well as identical twins. In all his results, no two ears were indistinguishable; leading him to state that ear shape can be used as a unique feature for identification purposes (Iannarelli, 1989). This is of great interest to forensics and security where both verification (is this the same person?) and identification (who is this person?) of people is often required. Therefore, much like fingerprint and face recognition (Smeets et al. 2010, 2012), ear recognition (Chen & Bhanu, 2007; Yan & Bowyer, 2007; Abaza et al. 2013) is an active field of research in biometrics (biometric authentication). From this perspective, bilateral symmetry of the human pinnae is also interesting, most obviously because the left ear of an individual can be used as a probe (test subject with unknown identity) in a comparison with a gallery of right ears (database of candidates with known identity) (Abaza & Ross, 2010). This way, smaller galleries can be used, containing one instead of two ear images per subject, with the associated reduction in maintenance costs. Furthermore, it better allows the application of ear recognition under unconstrained conditions (e.g. train station or airport), in which one has no control over whether the left or right ear can be captured and compared.

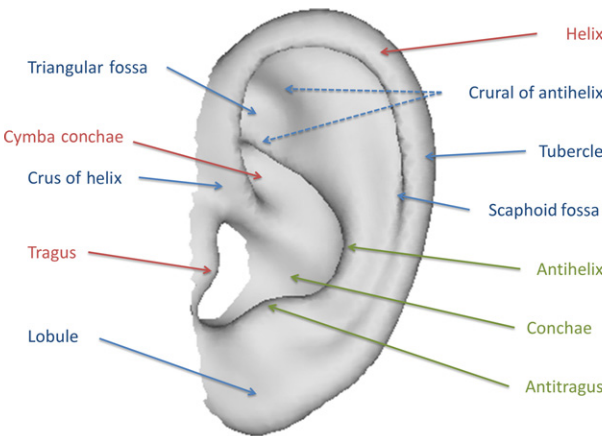

Fig. 1 The anatomy of the human pinna, which develops from six auricular hillocks (Abaza & Ross, 2010; Abaza et al. 2013). The first arch develops into the tragus, cymba conchae, and helix (red arrows), and the second arch develops into the antitragus, antihelix, and conchae (green arrows).

From an anatomical view, the type of bilateral symmetry observed is known as *matching symmetry* between paired structures that are present as separate mirror copies on both sides of the body (Klingenberg & McIntyre, 1998; Mardia et al. 2000; Klingenberg et al. 2002). During development, imbalances in growth will inevitably result in deviations from perfect symmetry (Hamada et al. 2002). These departures from symmetry, known as asymmetry, generate differences in ear shape between left and right, which are also referred to as intra-subject (in contrast to inter-subject) differences in this work. Although departures from symmetry are a property of the individual, patterns of asymmetry are studied at the level of the (sub)sample and are grouped into three categories, directional asymmetry, fluctuating asymmetry, and antisymmetry (Palmer & Strobeck, 1986; Palmer, 1994).

Whether the presence of asymmetry influences our capability in sound localization is unknown, but it is not unlikely to influence ear recognition based on matching symmetry. Investigations like these require the quantification of patterns of 3D ear shape variation in function of symmetry and asymmetry. This work, to the best of our knowledge, presents the first such systematic structural investigation in 3D. Building on previous work that focused on the decomposition of 3D facial shape into object (instead of matching) symmetry and asymmetry (Claes et al. 2012b), we use 3D spatially dense geometric morphometrics to decompose and investigate matching symmetry and asymmetry in the human pinnae. In doing so, valuable anatomical insights with possible implications mainly for ear recognition, but also sound localization, are gained and discussed. Additionally, some of these insights are demonstrated and again discussed in both a biometric verification and identification test setup.

Materials and methods

Sampling, mapping, and Procrustes superimposition

In all, 411 computer tomography (CT) angiograms from 411 different subjects (thus one image per subject) of the neck and brain were queried from a database of clinical 3D CT images. A subsample of 340 CT images, properly displaying a full head containing both ears without visible distortions (due to scanning positioning or aids such as pillows), was further selected. The subsample contains similar numbers of males (178) and females (162), with an average age of 52 ± 20 years (standard deviation), with a minimum age of 15 years and a maximum age of 89 years. A small set of 76 images were acquired using a Siemens Sensation 16, while the rest of the images were acquired using a Siemens Sensation 64. CT images were processed in MEVISLAB (MevisLab), where they were resampled to isotropic $1 \times 1 \times 1$ mm voxels. Subsequently, complete head surfaces were extracted using simple thresholding (-424 HU) of voxel intensities in combination with marching cubes (Lorensen &

Cline, 1987). Both left and right ears were extracted separately from each head using a bounding box-based manual selection procedure. Segmented ear surfaces were further cleaned by manually removing middle and inner ear structures. Right ear surfaces were reflected by changing the sign of the *x*-coordinate (Klingenberg & McIntyre, 1998; Mardia et al. 2000). In the remainder of the manuscript, when talking about the right ear, we refer to this reflected version unless otherwise stated.

A single left ear was randomly selected as the initial anthropometric mask (AM) for the ear shape, similar to what was done with facial shape in previous work (Claes et al. 2011, 2012a). In that work, facial surface scans before and after surgical treatment (Claes et al. 2012a) or expressing abnormal asymmetry (Claes et al. 2011) were analyzed using an AM that essentially generates the ability to compare different 3D images anatomically. The AM for ear shape used in this work was densely resampled with 4537 quasi-landmarks distributed uniformly and equidistantly across the shape region of interest using the remeshing function of the FastRBF toolbox in MATLAB™ (FastRBF). The AM surface comprised 7310 triangles with similar edge lengths (average edge length 1.21 mm $\pm$ 0.23 standard deviation) connecting neighboring quasi-landmarks. The AM served as a surface template and was non-rigidly mapped onto all 680 (left and right combined) ear surfaces. Basically, the AM represents the definition of the points or landmarks used in the investigation and the non-rigid mapping using 3D surface registration techniques comprises the indication of these points on all shapes (Appendix 1: Shape analysis using 3D surface registration). The result is that each shape in the database is now represented with the same number of quasi-landmarks and pattern of triangle connectivity. After a single mapping run over the complete database, the average quasi-landmark configuration was computed and used as an update to the AM. The whole process was repeated three times to reduce bias from the originally selected ear serving as AM. The AM used in the last run is seen in Fig. 1.

Subsequently, following Mardia et al. (2000), we performed a generalized Procrustes superimposition (Rohlf & Slice, 1990), eliminating differences in position, orientation, and scale of all left and right ears pooled. In the superimposed space, the Euclidean distance between two landmark configurations of Procrustes coordinates is known as the Procrustes distance and serves as a measure of shape difference or dissimilarity (Bookstein, 1991). Given paired left and right ears of the same subject after superimposition, an individual's ear shape can be separated into its symmetric and asymmetric part (Mardia et al. 2000). Indeed, partitioning of variation into symmetric variation and asymmetric variation among individuals uses averages and differences of those paired configurations (Klingenberg et al. 2002; Kimmerle & Jantz, 2005). Asymmetric variations imply differences between left and right ears within the same subject. Thus these are intra-subject variations and are created by taking the difference of paired left and right ears. The symmetric variations, on the other hand, are differences across different individuals after first averaging left and right ears within each subject. Thus these are inter-subject shape variations and are created by first taking the average of paired left and right ears.

Partitioning of pinna shape variation

Partitioning of pinna shape variation into symmetry and asymmetry was done following previous work to which the reader is referred for a detailed explanation (Claes et al. 2012b). In summary, the commonly used two-factor ANOVA design with individuals (rows) and left/right or side (columns) as the main effects was employed (Klingenberg et al. 2002). Variation in symmetry, corrected for the effects of asymmetry, is obtained from the main effect of individuals. Directional asymmetry (DA) corresponds to the main effect of side and fluctuating asymmetry (FA) is ascertained by the interaction term (individual $\times$ side). Measurement error is normally taken into account using a two-factor ANOVA with repeated measures of both factors in cells. The lack of repeated measures, and thus having a single measurement per cell, was dealt with in two different ways: noise injection (or simulating technical replication) and additive main & multiplicative interaction (AMMI) modeling.

The noise injection (technical noise level = 0.0104 after size normalization, obtained by multiple non-rigid mappings on a subset of ears, data not shown) generated three randomly perturbed replicate measurements needed for the traditional two-factor ANOVA partitioning. This was done under an isotropic model assumption with an appropriate number of degrees of freedom as defined for matching symmetry (Klingenberg & McIntyre, 1998). In this way we computed an overall and localized (per quasi-landmark) F statistic for the effect of symmetry, which is essentially coding for inter-subject variations, as well as the effect of directional and fluctuating asymmetry, which is essentially coding for intra-subject variations. It should be noted that the isotropic model assumption is restrictive, such that the interpretation of localized results should be done with caution, as mostly advised in the case of Procrustes-based analyses.

The AMMI framework provides an alternative when dealing with a single measurement per cell as well as a practical foundation when dealing with spatially dense data, and was used for partitioning and visualizing multivariate patterns of both symmetry and asymmetry as follows:

1. Taking the mean for each row creates an average ear shape from both sides for each individual. Subsequently, these coded for patterns of symmetry, which were then further modeled using principal component analysis (PCA).
2. The difference in column equals the average of all left ears subtracted from the average of all right ears and then coded for directional asymmetry.
3. Pairwise differences taken between sides for each row create the asymmetry component for each individual. Subsequently, these coded for patterns of asymmetry, which again were modeled with PCA after first centering (on the average) of the differences. The last is the same as subtracting DA from each individual asymmetry component.

For visualization purposes, the overall consensus ear configuration was re-added to the pairwise column differences after centering. The whole approach is related to the partitioning of shape variations in the works of Mardia et al. (2000) and Klingenberg et al. (2002) as outlined in Claes et al. (2012b).

Shape subspace comparison

Different groups (for example left and right ears seen as separate groups) may or may not occupy distinct loci and therefore span a different subspace in shape space. The idea is that, if two groups span the same subspace and share the same center or location, both groups will show great similarity in shape variations and it will be hard to separate members in one group from the other. In Appendix 2, we tested the differences in group location (differences in mean shape), variance–covariance scale [differences in dispersion (magnitude without direction) around the mean shape], and orientation (differences in variance directions around the mean shape).

First, the subspaces of left and right ears as distinct groups were compared to see whether shape patterns of left ears are different from those of right ears. Secondly, we compared the subspaces of intra- vs. inter-subject variations to see whether differences between left and right ears within individuals differ from the differences across the average ears of individuals. Both inter- and intra-subspaces were obtained using the AMMI modeling explained earlier.

Finally, all tests were performed in MATLAB™ (2012a) with 10 000 permutations. The permutations adapted to deal with paired data setups where appropriate.

Biometric verification and identification

The key element for the establishment of identity is a measure of similarity between biometric samples (Jain & Li, 2005; Jain et al. 2007). Given a biometric sample with unknown identity (probe), a measure of similarity is computed between this probe and possible candidate samples with known identities. In verification mode, a one-to-one comparison with a single candidate is performed and the identity is verified if the measure of similarity is deemed high enough. The performance of the verification mode used is evaluated using an ROC (receiver operating characteristic) curve analysis (Jain & Li, 2005; Jain et al. 2007). For a range of thresholds on the measure of similarity, the false accept fraction is plotted against the false reject fraction. A characteristic and often reported point on the curve is the equal error rate (EER), where the fractions of false accept and reject are equal. A lower EER indicates a better performance (Jain et al. 2007). In (closed set) identification mode, a one-to-many comparison with multiple candidates in a gallery is performed and identity is established by looking at the most similar candidates after sorting the gallery from highest to lowest likeness. The performance in identification mode is evaluated using cumulative match characteristic (CMC) curves (Jain & Li, 2005; Jain et al. 2007). These curves plot the cumulative identification rate in function of rank, which is simply the index of the true candidate in the sorted gallery list. To reduce the effect of gallery size (number of subjects), identification performance is plotted as a percentage of rank (Jain & Li, 2005). Identification performance is most often summarized with rank 1 identification rate (Jain & Li, 2005), reflecting the percentage of perfect recognition results. The higher the rank 1 identification rate, the better the performance.

In this work, 3D ear shapes were used as biometric samples and the Procrustes distance was used as measure of similarity between them. The 340 left ears, one-by-one, served as probes and the 340 right ears as the gallery. In doing so, 340 trials tested the presence of matching symmetry in the human pinnae for its ability to enable biometric authentication. Firstly, the complete shape of ears was used to compute Procrustes distances. Subsequently, using a range of thresholds on the localized F-ratio obtained from the effect of individuals corrected for asymmetry (using the noise-injected two-way ANOVA partitioning of shape) subsets of quasi-landmarks in ear shape were selected and used to compute Procrustes distances. The range of thresholds on the F-ratio went from the lowest to the highest observed F-ratio value in 10 equidistant steps. The idea was to focus on substructures in ear shape with increasing minimum ratios of inter- vs. intra-subject variation. In other words, pinna substructures with greater amounts of matching symmetry relative to their asymmetric variation were selected. Performance was evaluated in verification and identification mode using EER scores and rank 1 identification rates, respectively.

Results

Pinna shape decomposition

The two-factor ANOVA partitioning of external ear shape based on injected noise is given in Fig. 2. The mean squares (MS in first column) reflect effect magnitude and the F-ratios (second column) reflect relative magnitude or effect strength. Overall, the main effects of individuals, sides, and the interaction were significant ($P < 0.001$). Focusing on the first column, the inter-subject/symmetry variations (first row) were located mainly in the lobule, tragus, and tubercle or posterior part of the helix. To a lesser degree, variations among individuals were seen in the conchae, antitragus, antihelix, and remaining parts of the helix. Interestingly, variations in fluctuating asymmetry (third row) were also located in the lobule, tragus, and posterior part of the helix. These substructures typically 'stick out'/protrude and might therefore be more susceptible to developmental instabilities. Another result of interest is the observation of symmetry variation in the context of fluctuating asymmetry, which is depicted in the first row, 2nd column, or the F-ratio for matching symmetry. Here we see that the conchae, antitragus, and antihelix show greater symmetric than asymmetric variation. In other words, the differences across individuals are larger than the differences between the left and right sides for these substructures. Therefore, these regions might be favorable for identification as well as genetic variability. The effects of individuals as well as the effects of FA were significant across all the quasi-landmarks (third column). Some directional asymmetry (second row) was observed in the anterior part and the crus of the helix with additional small patches on the antitragus and lower posterior part of the helix. As expected, the error term was visually evident as a fuzzy diffuse pattern consistent with the noise injection process.

From the AMMI framework, the first three PCs modeling patterns of symmetry (inter-subject) and FA (intra-subject) separately are given in Fig. 3. We observe from these images that the three PCs coding for inter-subject variations have a greater effect in magnitude compared with the PCs coding for intra-subject variations. In correspondence with the observations made in Fig. 2, substructures such as the lobule, tragus, and posterior part of the helix are affected in both inter- and intra-subject PCs. Also corresponding to Fig. 2, the conchae, antihelix, and antitragus are affected more in the inter-subject patterns. The correspondences between Figs 2 and 3 were as expected, as both techniques focus on similar shape decompositions. However, the results in Fig. 2 are only based on the distances of changes in 3D of the quasi-landmarks treated as univariate variables. In contrast, the results in Fig. 3 capture multivariate patterns of covariance in the 3D displacements separately from the quasi-landmarks. It should be noted that although PCA is a

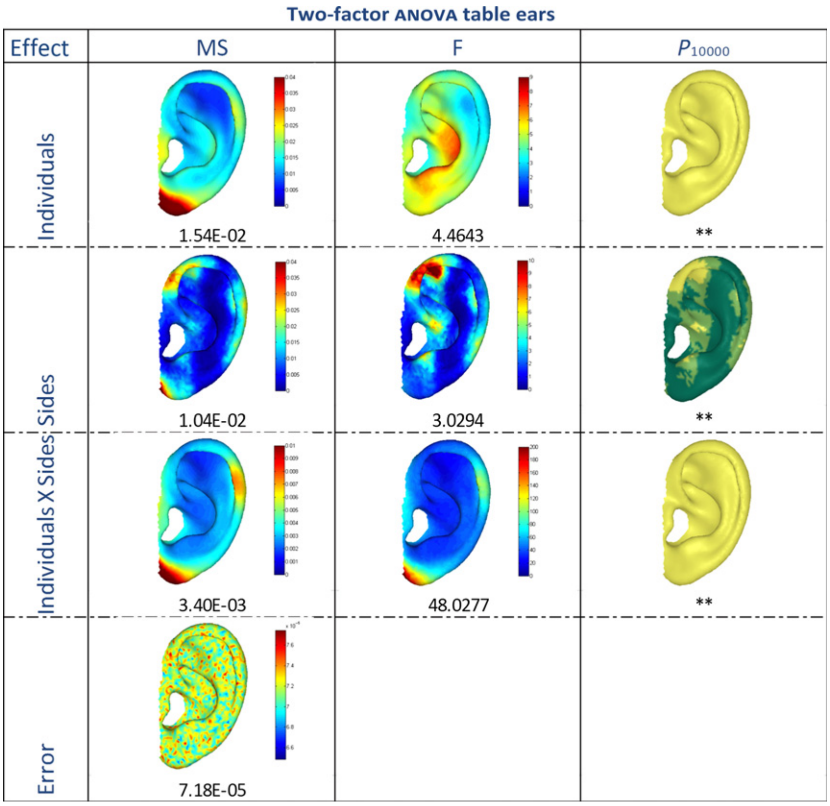

Fig. 2 Two-factor ANOVA partitioning of ear shape variation following an isotropic model with injected noise. *P*-values using 10 000 permutations with ** and yellow $P < 0.001$; * and light green $P < 0.05$; dark green not significant ($P \geq 0.05$). MS, mean square, is the sum of squares divided by the appropriate degrees of freedom, reflecting the magnitude of the effect. F, F-ratio, is the MS divided by an appropriate error MS, reflecting the relative magnitude or strength of the effect (effect-size).

practical tool in modeling patterns of covariance and allows some comparisons to be made, as in this work, it is best to avoid assigning any further biological meaning or insight to them individually.

The results on comparing shape subspaces are given in Appendix 2. Left and right subspaces covered the same loci in shape-space. In other words, similar shape patterns occur in left and right ears. In contrast, the differences between paired left and right ears expressed lower dispersion and are dissimilar in covariance structure compared with differences across individuals. In other words, it should be possible to identify individuals based on matching symmetry, even in the presence of asymmetry, because the differences across individuals are larger and often different than the differences between left and right.

Biometric evaluation based on matching symmetry

In the previous results we clearly observed both symmetry as well as asymmetry in the human pinna. In the remainder of the results, the idea is to test to what extent this approach can be exploited in biometric verification and identification setups. The minimum and maximum localized F-ratio (per quasi-landmark) in Fig. 2, column two, row one, was 2.4 and 7.7, respectively, from which the following series of F cutoffs was extracted: 2.4, 2.9, 3.4, 4, 4.5, 5, 5.6, 6.1, 6.6, and 7.2. For each of these cutoffs, quasi-landmarks with equal or greater localized F-ratio were selected. As such, a cutoff of 2.4 yields 100% of quasi-landmarks and increasing the cutoff implied a selective reduction as depicted in Fig. 4. Using all quasi-landmarks, the EER was equal to 14%, with a rank 1 identification rate of 79%. Increasing the cutoff improved both the verification and identification performance. A 'best' cutoff was reached at 4.5 with an EER and rank 1 identification rate of 11 and 81%, respectively. A further increase in cutoff resulted in a steep drop in performance. These results indicate that it is sensible to focus on substructures expressing a higher F-ratio in inter- vs. intra-subject variation in a biometric setup based on matching symmetry. According to the 'best' cutoff, the focus is mainly on the conchae, antitragus, and antihelix, with additional patches from the tragus, lobule, triangular fossa, and anterior part of the helix. A further increase in cutoff leads to loss of 'enough' shape information, leaving no more useful information to individualize.

Discussion

The human external ear, or pinna, shows both a highly variable convoluted shape and bilateral symmetry. It is somewhat counterintuitive to have a shape with very specific functions, namely capturing, amplifying, and filtering incoming sound, that also shows so much inter-individual variation as to be unique for every individual. Some aspects of shape variation in the human ear have been known for over a century and have been used (correctly or not) by 19th

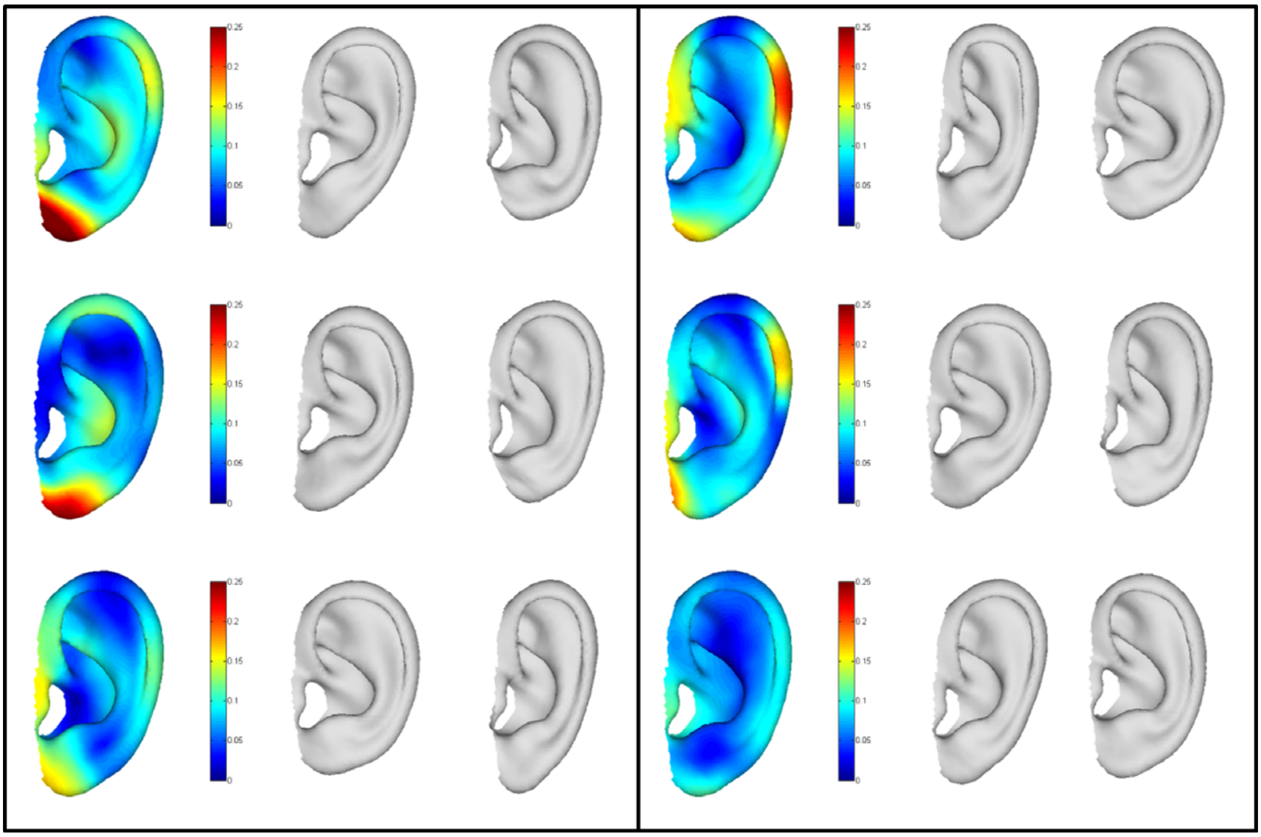

Fig. 3 The effects (colored ears), a positive morph (first ear shape) and a negative morph (second ear shape) along the first three principal components (rows 1–3) in multivariate patterns of inter-subject (left) and intra-subject variations (right) obtained from the AMMI framework for shape decomposition.

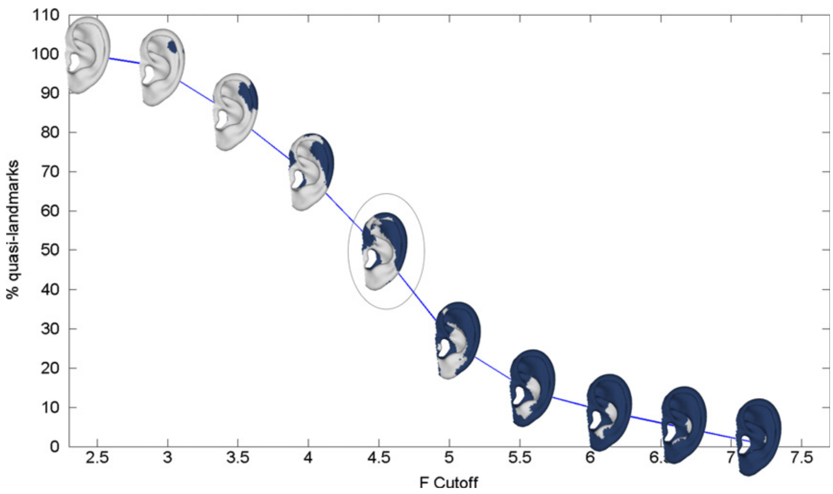

Fig. 4 Percentage and location of quasi-landmarks in ear shape selected (white zones in ear images) as a function of the F-ratio threshold. The best identification performances are obtained with the configuration encircled.

century physiognomists (Beard, 1978). Our presentation here is the first systematic 3D investigation of matching symmetry in the human pinnae from an anatomical perspective. We have extended our previous work using spatially dense geometric morphometrics to quantify human facial variation (Claes et al. 2011, 2012b). We used the familiar two-way ANOVA to decompose outer ear shape into symmetry and asymmetry. We found substantial levels of matching symmetry in all substructures of the pinna anatomy. The inter-subject or symmetry variations were mainly located in the lobule, tragus, and tubercle or posterior part of the helix. To a lower degree, variations among individuals were also seen in the conchae, antitragus, antihelix and remaining parts of the helix. However, the lobule, tragus, and tubercle part of the helix are ear substructures that tend to 'stick out' and they clearly demonstrated the highest degree of asymmetry besides matching symmetry in ear shape. This is similarly seen for protruding facial features such as the nose (Claes et al. 2012b). It was therefore concluded that the conchae, antitragus, and antihelix, in contrast to the lobule, tragus, and tubercle part of the helix, might be favorable regions for the purpose of identification, as was subsequently demonstrated in this work. Coincidence or not, these three substructures developmentally all originate from the second arch of auricle hillocks (green arrows in Fig. 1). In the remainder of this section we focus on the discussion of these results in the context mainly of biometrics and sound localization.

The uniqueness in shape of the human pinna as led to its use as a biometric identifier (Iannarelli, 1989; Jain et al. 2004; Yan & Adviser-Bowyer, 2006) and this is often compared to face recognition (Victor et al. 2002; Chang et al. 2003). Anatomically, ear recognition has two main advantages. Firstly, ear shape is quite stable throughout the lifespan (Iannarelli, 1989). Second, ear shape does not change like facial shape due to facial expressions (Smeets et al. 2010). A recent survey on ear biometrics (Abaza et al. 2013) lists 2D as well as some 3D ear image databases. In contrast to this work, 3D information in these databases was captured using surface range scanners. Due to the amount of radiation involved, using a CT scanner to collect research data is unethical. Although CT scanners are too dangerous and expensive to use in security systems, the greater quality in 3D shape needed for anatomical studies is not available in contemporary laser range scanners. Therefore we used a database of patients undergoing diagnostic CT scanning. Furthermore, it is not unlikely that the resulting AMMI models from the 340 scans, which are geometrically of high quality, can be used in future model-based ear biometric approaches, for which the authors can be contacted.

As outlined by Abaza et al. (2013), ear symmetry is mentioned as a feature to be exploited in the design of future recognition systems. A few published papers on ear biometrics (see Table 1) have incorporated an investigation of ear symmetry using the ears on one side of the head as a gallery and the other side as probes (Yan & Bowyer, 2005, 2007; Abaza & Ross, 2010). In contrast to this work, those investigations were from a pure biometric perspective only. Furthermore, their goal was not to find or focus on any particular substructures of interest, but just to see to what extent ear symmetry, if present, can be used to identify people. Their results should be compared with our results obtained using complete ear shape. However, an in-depth comparison is not straightforward. Firstly, as previously mentioned, this study started from high quality 3D data obtained from a medical CT scanner. Second, results are influenced by the choice of similarity measure. In this work the Procrustes distance was used, but alternative measures of similarity exist and are an active topic of investigation in biometrics in general (Jain et al. 2007). Finally, our main purpose was to investigate matching symmetry from an anatomical perspective using spatially dense geometric morphometrics. In addition, the aim was to illustrate the benefit of incorporating this knowledge appropriately. We distinguished areas that are relatively less or more selective in establishing identity based on matching symmetry. This has been put to the test in a biometric verification and identification setup. By focusing on substructures with higher F-ratios (selected using thresholding) an increase in biometric performance was observed, until the selection became too small for further improvement.

The ears have been endowed with their complex morphology to suit the task of echolocation. But if the ear morphology has been optimized for this task, it seems contradictory that there is such a large variability in ear morphology across the human population. On the other hand, psychoacoustic localization experiments do show that there is a large variability in the human ability to localize sounds in front/back and up/down dimensions (Wightman & Kistler, 1989b; Wenzel et al. 1993; Zahorik et al. 2006). Some listeners outperform others by a factor of 20 in a front/back localization task (Wenzel et al. 1993), and the mean localization error in the up/down dimension can range between 5° and 40°, depending on the listener (Wenzel et al. 1993). A possible explanation may lie in the differences in ear morphology: some listeners' outer ears may provide more prominent cues, allowing better spatial localization. This hypothesis was tested in two different

Table 1 Short overview of related methods in ear biometrics testing matching symmetry in ear shape and their performances on verification and identification testing.

Reference	Method	Rank 1 identification in %	Equal error rate (EER) in %
Yan & Bowyer (2005, 2007)	3D ICP	90	Na
Abaza & Ross (2010)	12 Iannarellis measurements	Na	16.75
Abaza & Ross (2010)	Shape from shading (Cadavid & Abdel-Mottaleb, 2008)	49	17.06
Abaza & Ross (2010)	Eigen Ear (Chang et al. 2003)	35.31	21.05

studies (Andéol et al. 2013; Majdak et al. 2014) and their results suggest that it is not so much the exact morphology of the ear (an acoustic factor) that determines sound localization performance, but the individual's ability to detect spectral cues (a perceptual factor) (Drennan & Watson, 2001; Eddins & Bero, 2007).

In addition to variation in ear shape variation among individuals, the left and right ears are not exact mirror copies. This departure from matching symmetry does not automatically have an negative effect on sound localization. On the contrary, pinna asymmetry may even improve sound localization, as seen in some birds (Norberg, 1977; Takahashi, 2010). Bilateral asymmetry has evolved independently at least five times among owls and is achieved by a variety of morphological adaptations, from the skull to the soft tissues of the outer ears (Volman, 1994). This asymmetry helps the owl to localize prey in the vertical direction, complementing inter-aural time difference as a cue to estimate the horizontal position. To what extent such a bilateral asymmetry may be beneficial for human sound localization remains, as far as we know, uninvestigated. But the fact that it is not a systematic feature in humans, together with the finding that the exact ear shape does not appear to be that important (Andéol et al. 2013; Majdak et al. 2014), suggests that matching symmetry does not play a significant role in human sound localization.

Given the evidence of a limited role for human ear shape left/right asymmetries in sound localization, leaves the question of why our ears show such levels of matching symmetry. One could speculate that the primary driver behind bilateral ear symmetry in humans is sexual selection, as persons who have lower FA (less asymmetry) are associated with better environments and 'genetics' (Hume & Montgomerie, 2001). The lower levels of FA likely result from lower levels of developmental instability as compared with persons with higher levels of ear FA. However, it is easy to assume that left and right deviations from symmetry are in fact expressed more in the face, and probably hands and feet. This because the ear is mainly cartilaginous tissue, whereas face/hand/feet are under strong structural and functional influence of underlying muscular tissue and its neural control, which tend to have left and right biases. Interesting follow-up studies should include the relationship of FA across different parts of the human body. Nevertheless, there are a number of congenital dysmorphologies, such as Treacher Collins, that involve the external ear. The patterns of malformation of the ear involve the positioning (vertical, horizontal, and rotation), size across several dimensions, and shape, and are commonly used as diagnostic criteria (Jones et al. 2013). The anatomical findings and spatially dense methods that we present here provide the basis for further investigations into both normal range and clinically manifest ear shape variation. Although, as mentioned above, CT-based datasets, like the one we used, are not expected to become readily available, high-resolution scans like these can provide a means by which to scale and validate lower resolution scanning like laser scanning and photogrammetry. This would make possible studies of many more individuals from more populations, as well as relationship modeling of genotypes from phenotypes using methods like recently described bootstrap response-based imputation modeling (BRIM) (Claes et al. 2014).

In recent years, efforts have been made to include audio in the virtual reality experience (Carlile, 1996). Virtual auditory space (VAS) technology introduces HRTFs to the signals presented over headphones and this way a listener can be placed in any kind of auditory environment. However, the individual differences in ear morphology and their respective HRTFs are too large to use generic, non-individualized filters: a slightly different HRTF would severely hamper correct sound localization and would result in front/back up/down errors (Wenzel et al. 1993; Carlile, 1996). Although measuring the individual HRTF of each user would yield the best results, this is not feasible for large-scale projects and commercial endeavors, given the specialized facilities and time required. For this reason, researchers have been working to find other ways to model an individual's HRTF (for an overview, see Xu et al. (2007). A promising alternative to obtain an individual's HRTF is via acoustic simulation based on the individual's ear morphology. If one knows the ear shape, for example modeled using the framework presented here, it is possible to simulate how it would interact with sound coming from different directions and to calculate the corresponding HRTF (Otani & Ise, 2006). This way the crux of the problem is shifted to the assessment of the complex ear morphology at the individual level. The basis of modeling shape variations derived in this study may facilitate this essential step, and may allow one to estimate an individual's HRTF using ear shape information.

Conclusion

Matching symmetry is observed in the human pinnae. However, during development in vertebrates, imbalances in growth will inevitably result in deviations from perfect symmetry, known as asymmetry. We present here a 3D investigation of both asymmetry and matching symmetry in the human pinnae. Matching symmetry was observed in all anatomical substructures of the pinna. However, substructures that 'stick out', such as the helix, tragus, and lobule, also show a fair degree of asymmetry. In contrast, substructures such as the conchae, antitragus, and antihelix show more matching symmetry than asymmetry. The results and the methods employed have important implications on future investigations and applications in ear recognition and sound localization. Since we show that in the vast majority of cases, the left ear of an individual can be compared as a probe in a gallery of right ears, biometric comparisons can be generalized in cases where only one ear is visible. In this context we also demonstrated improved biometric verification and identification using the anatomical insights gained. The present investigation brings future recognition systems one step closer to operating in unconstrained environments such as train stations and airports. Other implications involve the resulting models coding for patterns of variation in ear shape obtained from 340 CT scans, which are geometrically of high quality. These can be used not only to help improve other 3D ear models but also to allow shape variation to be simulated and tested explicitly for a variety of experiments, for example in sound localization, and genetic and environmental effects on ear variation. Furthermore, given the spatially dense nature of these methods, explicitly modeling individual ear shape provides a promising alternative to measuring an individual's HRTF.

Acknowledgements

This work is supported by the Flemish Institute for the Promotion of Innovation by Science and Technology in Flanders (IWT Vlaanderen), the Research Program of the Fund for Scientific Research – Flanders (Belgium) (FWO), the Research Fund KU Leuven.

Conflict of interest

The authors declare no conflict of interest.

Author contributions

P.C. developed the technical algorithms, implemented the statistical routines, designed and performed the data analysis, and wrote the manuscript with appropriate input and revisions from all other authors. J.R. contributed the insights and discussion on ear morphology in the context of sound localization, and M.D.S. did the same from a genetic evolutionary perspective.

References

Abaza A, Ross A (2010) Towards understanding the symmetry of Human ears: A biometric perspective. In: 4th IEEE International Conference on Biometrics: Theory, applications and systems (BTAS). Washington, DC.

Abaza A, Ross A, Hebert C, et al. (2013) A survey on ear biometrics. *ACM Comput Surv*, **45**, 22:1–22:35.

Andéol G, Macpherson EA, Sabin AT (2013) Sound localization in noise and sensitivity to spectral shape. *Hear Res* **304**, 20–27.

Anderson MJ (2001) A new method for non-parametric multivariate analysis of variance. *Austral Ecol* **26**, 32–46.

Anderson MJ (2006) Distance-based tests for homogeneity of multivariate dispersions. *Biometrics* **62**, 245–253.

Andresen PR, Bookstein FL, Conradsen K, Ersboll BK, Marsh JL, Kreiborg S (2000) Surface-bounded growth modeling applied to human mandibles. *IEEE Transactions on Medical Imaging* **19**(11), 1053–1063.

Beard JS (1978) The physiognomic approach. In: *Classification of Plant Communities*. (ed. Whittaker R. H.), pp. 33–64. Netherlands, The Hauge: Springer.

Besl PJ, McKay ND (1992) A method for registration of 3-D shapes. *IEEE Trans Pattern Anal Mach Intell* **14**, 239–256.

Blauert J (1997) *Spatial Hearing: The Psychophysics of Human Sound Localization*. Hong Kong: MIT Press.

Bookstein FL (1991) *Morphometric Tools for Landmark Data: Geometry and Biology*. Cambridge: Cambridge University Press.

Bookstein FL (1997) Shape and the information in medical images: a decade of the morphometric synthesis. *Comput Vis Image Underst* **66**, 97–118.

Cadavid S, Abdel-Mottaleb M (2008) 3-D ear modeling and recognition from video sequences using shape from shading. *IEEE Trans Inf Forensic Secur* **3**, 709–718.

Carlile S (1996) *Virtual auditory Space: Generation and Applications*. Austin: RG Landes.

Chang K, Bowyer KW, Sarkar S, et al. (2003) Comparison and combination of ear and face images in appearance-based biometrics. *IEEE Trans Pattern Anal Mach Intell* **25**, 1160–1165.

Chen HS, Bhanu B (2007) Human ear recognition in 3D. *IEEE Trans Pattern Anal Mach Intell* **29**, 718–737.

Claes P (2007) *A Robust Statistical Surface Registration Framework Using Implicit Function Representations: Application in Craniofacial Reconstruction. Thesis.*. Leuven: K. U. Leuven, Faculteit Ingenieurswetenschappen, Department Elektrotechniek, afdeling PSI.

Claes P, Walters M, Vandermeulen D, et al. (2011) Spatially-dense 3D facial asymmetry assessment in both typical and disordered growth. *J Anat* **219**, 444–455.

Claes P, Walters M, Clement JG (2012a) Improved facial outcome assessment using a 3D anthropometric mask. *Int J Oral Maxillofac Surg* **41**, 324–330.

Claes P, Walters M, Shriver MD, et al. (2012b) Sexual dimorphism in multiple aspects of 3D facial symmetry & asymmetry defined by spatially dense geometric morphometrics. *J Anat* **221**, 97–114.

Claes P, Liberton DK, Daniels K, et al. (2014) Modeling 3D facial shape from DNA. *PLoS Genet* **10**, e1004224.

Drennan WR, Watson CS (2001) Sources of variation in profile analysis. I. Individual differences and extended training. *J Acoust Soc Am* **110**, 2491–2497.

Dryden IL, Mardia KV (1998) *Statistical Shape Analysis*. New York: John Wiley & Sons.

Eddins DA, Bero EM (2007) Spectral modulation detection as a function of modulation frequency, carrier bandwidth, and carrier frequency region. *J Acoust Soc Am* **121**, 363–372.

FastRBF FarField Technology by ARANZ Ltd. http://www.farfieldtechnology.com/.

Giachetti A, Mazzi E, Piscitelli F, et al. (2014) *SHREC'14 Track: Automatic Location of Landmarks used in Manual Anthropometry* 93–100.

Goodall C (1991) Procrustes methods in the statistical analysis of shape. *J R Stat Soc Ser B* **53**, 285–339.

Hamada H, Meno C, Watanabe D, et al. (2002) Establishment of vertebrate left-right asymmetry. *Nat Rev Genet* **3**, 103–113.

Hamm J, Lee DD (2008) Grassman Discriminant Analysis: a Unifying View on Subspace-Based learning. In Proceedings of the 25th International Conference on Machine Learning, pp. 376–383. Helsinki: ACM.

Hume DK, Montgomerie R (2001) Facial attractiveness signals different aspects of 'quality' in women and men. *Evol Hum Behav* **22**, 93–112.

Iannarelli A (1989) *Ear Identification*. Fremont: Paramount Publishing Company.

Jain AK, Li SZ (2005) *Handbook of Face Recognition*. New York: Springer-Verlag, Inc.

Jain AK, Ross A, Prabhakar S (2004) An introduction to biometric recognition. *IEEE Trans Circuits Syst Video Technol* **14**, 4–20.

Jain AK, Flynn P, Ross AA (2007) *Handbook of Biometrics*. New York: Springer-Verlag, Inc.

Jones KL, Jones MC, del Campo M (2013) *Smith's Recognizable Patterns of Human Malformation*. Philadelphia: Elsevier Health Sciences.

Kimmerle EH, Jantz RL (2005) Secular trends in craniofacial asymmetry studied by geometric morphometry and generalized Procrustes methods. In: *Modern Morphometrics in Physical Anthropology* (ed. Slice D), pp. 247–263. New York: Kluwer Academic/Plenum Publishers.

Klingenberg CP, McIntyre GS (1998) Geometric morphometrics of developmental instability: analyzing patterns of fluctuating asymmetry with Procrustes methods. *Evolution* **52**, 1363–1375.

Klingenberg CP, Barluenga M, Meyer A (2002) Shape analysis of symmetric structures: quantifying variation among individuals and asymmetry. *Evolution* **56**, 1909–1920.

Knyazev AV, Argentati ME (2002) Principal angles between subspaces in an A-based scalar product: algorithms and perturbation estimates. *SIAM J Sci Comput* **23**, 2008–2040.

Kranklin SB, Gibson DJ, Robertson PA, et al. (1995) Parallel Analysis: a method for determining significant principal components. *J Veg Sci* **6**, 99–106.

Krzanowski WJ (1979) Between-groups comparison of principal components. *J Am Stat Assoc* **74**, 703–707.

Lorensen WE, Cline HE (1987) Marching cubes: a high resolution 3D surface construction algorithm. *SIGGRAPH Comput Graph* **21**, 163–169.

Majdak P, Baumgartner R, Laback B (2014) Acoustic and non-acoustic factors in modeling listener-specific performance of sagittal-plane sound localization. *Front Psychol*, **5**, 319, 1–10.

Mardia KV, Bookstein FL, Moreton IJ (2000) Statistical assessment of bilateral symmetry of shapes. *Biometrika* **87**, 285–300.

McArdle BH, Anderson MJ (2001) Fitting multivariate models to community data: a comment on distance-based redundancy analysis. *Ecology* **82**, 290–297.

MevisLab (2014) *Medical Image Processing and Visualization Software*. Bremen: MeVis Medical Solutions AG.

Norberg R (1977) Occurrence and independent evolution of bilateral ear asymmetry in owls and implications on owl taxonomy. *Philos Trans R Soc Lond B* **280**, 375–408.

Otani M, Ise S (2006) Fast calculation system specialized for head-related transfer function based on boundary element method. *J Acoust Soc Am* **119**, 2589–2598.

Palmer AR (1994) Fluctuating asymmetry: a primer. In: *Developmental Instability: Its Origins and Implications* (ed. Markov T), pp. 335–364. Dordrecht: Kluwer.

Palmer AR, Strobeck C (1986) Fluctuating asymmetry: measurement, analysis, patterns. *Annu Rev Ecol Syst* **17**, 391–421.

Reijniers J, Vanderelst D, Jin C, et al. (2014) An ideal-observer model of human sound localization. *Biol Cybern* **108**, 169–181.

Richtsmeier JT, Deleon VB, Lele SR (2002) The promise of geometric morphometrics. *Am J Phys Anthropol* **45**, 63–91.

Rohlf F, Slice D (1990) Extensions of the procrustus method for the optimal superimposition of landmarks. *Syst Zool* **39**, 40–59.

Smeets D, Claes P, Vandermeulen D, et al. (2010) Objective 3D face recognition: evolution, approaches and challenges. *Forensic Sci Int* **201**, 125–132.

Smeets D, Claes P, Hermans J, et al. (2012) A comparative study of 3D face recognition under expression variations. *IEEE Trans Syst Man Cybern Part C Appl Rev* **42**, 710–727.

Snyders J, Claes P, Vandermeulen D, et al. (2014) Development and comparison of non-rigid surface registration and extensions, Technical Report: KUL/ESAT/PSI/1401. pp. 1–55.

Takahashi TT (2010) How the owl tracks its prey – II. *J Exp Biol* **213**, 3399–3408.

Van Valen L (1962) Study of fluctuating asymmetry. *Evolution* **16**, 125–142.

Victor B, Bowyer K, Sarkar S (2002) An evaluation of face and ear biometrics. In Proceedings 16th International Conference on Pattern Recognition, 2002, pp. 429–432.

Volman S (1994) Directional hearing in owls: neurobiology, behaviour and evolution. In: *Perception and Motor Control in Birds* (ed. Davies M.N.O. and Green P.R.), pp. 292–314. Berlin Heidelberg: Springer.

Wenzel EM, Arruda M, Kistler DJ, et al. (1993) Localization using nonindividualized head-related transfer functions. *J Acoust Soc Am* **94**, 111–123.

Wightman FL, Kistler DJ (1989a) Headphone simulation of free-field listening. I: stimulus synthesis. *J Acoust Soc Am* **85**, 858–867.

Wightman FL, Kistler DJ (1989b) Headphone simulation of free-field listening. II: Psychophysical validation. *J Acoust Soc Am* **85**, 868–878.

Xu S, Li Z, Salvendy G (2007) Individualization of head-related transfer function for three-dimensional virtual auditory display: a review. In: *Virtual Reality* (ed. Shumaker R.), pp. 397–407. Berlin Heidelberg: Springer.

Yan P, Adviser-Bowyer KW (2006) *Ear Biometrics in Human Identification*. PhD in computer science and engineering University of Notre Dame.

Yan P, Bowyer K (2005) Empirical evaluation of advanced ear biometrics. In: CVPR Workshops, IEEE Computer Society Conference on Computer Vision and Pattern Recognition-Workshops, 2005. pp. 41–41.

Yan P, Bowyer KW (2007) Biometric recognition using 3D ear shape. *IEEE Trans Pattern Anal Mach Intell* **29**, 1–12.

Zahorik P, Bangayan P, Sundareswaran V, et al. (2006) Perceptual recalibration in human sound localization: learning to remediate front-back reversals. *J Acoust Soc Am* **120**, 343–359.

Appendix 1

Shape analysis based on 3D surface registration

Landmarks or homologous points or points of correspondence on shapes that match between and within populations form the mathematical basis of a geometric morphometric-based shape analysis (Dryden & Mardia, 1998). 'True' landmarks have developmental, functional, structural or evolutionary significance (Richtsmeier et al. 2002) and often have been indicated manually on 2D as well as 3D images and shapes. These landmarks have a particular name and are uniquely defined. However, owing to the lack of anatomically discrete features in regions of the ear, manually indicated landmarks provide only a sparse representation and salient features of ear shape can be overlooked.

The demand to detect, quantify and visualize both subtle and severe asymmetries in discrete regions of the ear requires more complete spatially dense shape representations. As discussed in Claes et al. (2011), the biggest challenge when working with spatially dense shape representations is to obtain compatible landmark configurations beyond 'true' landmarks. Following the original and broad definition of semi-landmarks, that is, points that do not have names but that correspond across all cases of similar but variable shapes (Bookstein, 1997; Andersen et al. 2000), quasi- and semi-landmarks are essentially the same. The challenge for both types of landmarks is to find a mapping function that establishes one-to-one correspondences and therefore generates compatible configurations from one 3D ear shape to the other.

Finding a mapping function between two or more 3D shapes, without pre-assigned correspondences, is commonly known as '3D registration' in computer vision. The goal of a registration algorithm is to find the geometrical relationship (one-to-one correspondences) between 3D shapes following a predefined transformation model (Claes, 2007). A popular registration algorithm, without pre-assigned correspondences, is the iterative closest point (ICP) procedure (Besl & McKay, 1992). ICP is an iterative two-step algorithm in which candidate correspondences and transformation model parameters are updated until no more change in either is observed. The mapping strategy used here is a non-rigid (in contrast to rigid) extension of the original ICP algorithm. Iteratively, more flexibility in the elasticity (bending energy) of the transformation model is allowed such that initially larger, but gradually more local and subtler, shape differences are accommodated when searching for correspondences.

It is important to note that the development of 3D surface registration algorithms has been an active field of research in computer vision over the past two decades and that a different algorithm can lead to different mapping results. Recently, we implemented the most successful algorithms found in the literature while making additional improvements (e.g. speeding up computational time) and comparing them. Technical details and the comparative study of the non-rigid mapping used on human faces, skulls, and bodies can be found in Snyders et al. (2014) and Giachetti et al. (2014). From these results, the best performing algorithm using a combination of weighted K-nearest neighbors and a newly proposed visco-elastic deformation model was chosen to perform the required shape mappings in this work.

Appendix 2

Shape subspace comparison

The generalized Procrustes superimposition results in a tangent space of the Kendall shape space centered on the overall consensus configuration (Dryden & Mardia, 1998). All ear shapes represented as quasi-landmark configurations were superimposed on this tangent space. In previous work (Claes et al. 2012b) we provided a non-parametric D (istance)-statistic-based permutation framework based on the work of Anderson (2001, 2006, McArdle & Anderson, 2001), to test differences in group location, variance-covariance scale, and orientation. In summary: (i) The location test

Table A1 Results of left vs. right ear and inter vs. intra ear shape variations in group location, scale and orientation. pperm is *P*-value under permutation with 10 000 permutations. Dstat is the distance statistic used for the respective tests.

	Left–right		Inter–intra	
	Dstat	pperm	Dstat	pperm
Location	0.47	0.0003	0.47	0.0719
Scale	0.24	0.0007	0.48	0.0000
Orientation	0.05	0.1913	0.07	0.0030
	0.08	0.0757	0.10	0.0029
	0.10	0.0880	0.14	0.0000
	0.12	0.1222	0.17	0.0000
	0.14	0.2414	0.21	0.0000
	0.17	0.1090	0.25	0.0000
	0.20	0.0885	0.30	0.0000
	0.23	0.0752	0.34	0.0000
	0.26	0.1432	0.38	0.0000
	0.29	0.1813	0.42	0.0000
	0.32	0.1470	0.46	0.0000
	0.36	0.1095	0.51	0.0000
	0.39	0.1061	0.55	0.0000
	0.43	0.0702	0.59	0.0000
	0.47	0.0722	0.64	0.0000
	0.51	0.1219	0.69	0.0000
	0.56	0.0837	0.75	0.0000
	0.61	0.1242	0.80	0.0000
	0.65	0.2482	0.86	0.0000
	0.71	0.1287	0.92	0.0000
	0.77	0.1414	0.98	0.0000
	0.82	0.1921	1.04	0.0000
	0.88	0.2968	1.11	0.0000
	0.94	0.4440	1.18	0.0000
	1.01	0.5577	1.26	0.0000
	1.10	0.4090	1.33	0.0000
	1.19	0.3814	1.41	0.0000
	1.28	0.3449	1.51	0.0000
	1.40	0.2399	1.60	0.0000
	1.52	0.3395	1.69	0.0000
	1.66	0.4883	1.80	0.0000
	1.88	0.1807	1.92	0.0000
	2.10	0.1682	2.06	0.0000
	2.30	0.2830	2.19	0.0000
			2.34	0.0000
			2.51	0.0000
			2.68	0.0000
			2.84	0.0000
			3.01	0.0000
			3.17	0.0000

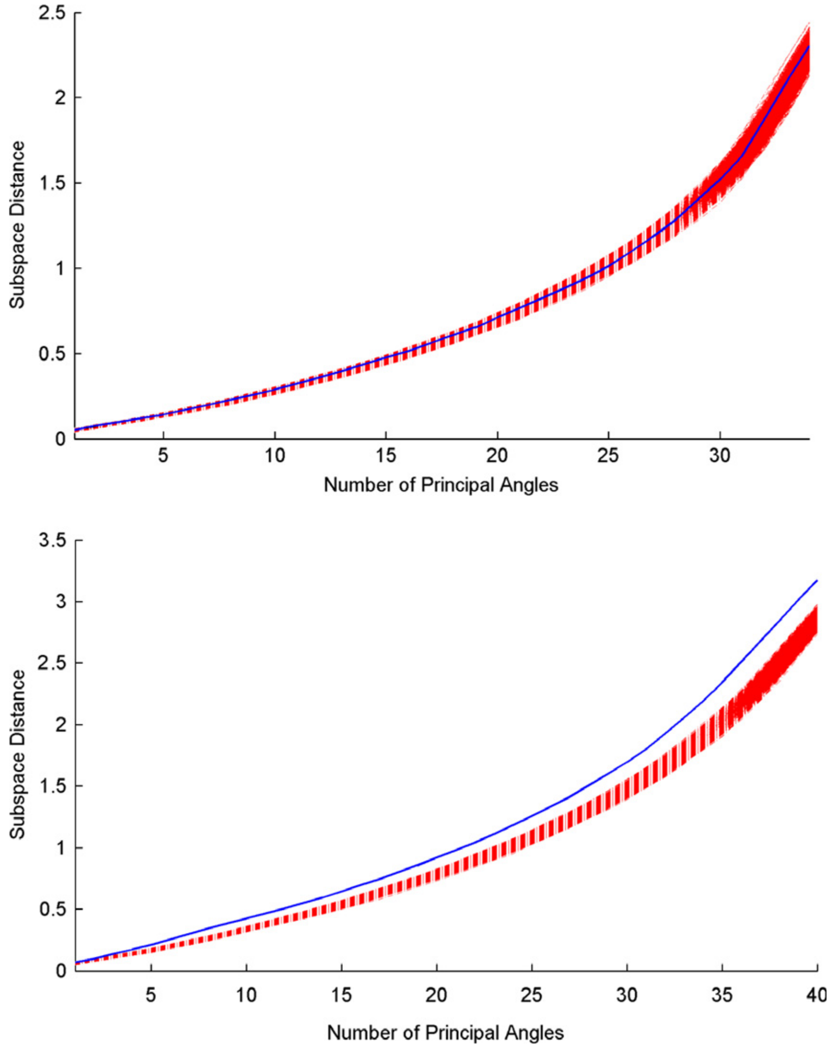

Fig. A1 Subspace differences on the aspect of population orientation with observed D-statistic (blue line) against the null distribution (red lines) obtained using permutation in function of the number of principal angles. Above, a non-significant difference between left and right ear subspaces (observed statistic is masked by the null distribution). Below, a significant difference between inter- and intra-subject ear variations (observed statistic is not masked by the null distribution).

assessed the difference in central tendency, which generally measures group divergence. The D-statistic employed was simply the Euclidean distance between sample means. (ii) The variance–covariance scale test assessed the difference in overall dispersion, which measures differences in the magnitude of variance or the stability of a group around its consensus configuration. The D-statistic used was the absolute difference in average residual of both groups. (iii) The 2variance–covariance orientation test assessed the difference in covariance structure, which measures differences in patterns or directions of variance. The D-statistic was constructed using the projection metric (Hamm & Lee, 2008) based on critical angles (Krzanowski, 1979), also known as principal angles (Knyazev & Argentati, 2002), between subspaces. These angles combine principal components (PCs) in a pairwise fashion from both subspaces in decreasing similarity or increasing angle value. The number of significant PCs to be used was determined using parallel analysis (PA) (Kranklin et al. 1995), which statistically defines spurious PCs compared with PCs of equally dimensioned but random and uncorrelated data. Note that alternative F-statistics to the respective D-statistics used here were provided as well (Claes et al. 2012b). However, they generated similar results and were computationally much more expensive and hence the results are not shown. Also note that similarities with parts of these tests and well-known tests in shape analysis exist (Claes et al. 2012b), such as the two independent sample Goodall's F-test (Goodall, 1991; Bookstein, 1997) and

Table A2 Parallel analysis (PA) results for left, right, inter- and intra-ear shape subspaces with percentage of the total variance explained by the number of significant principal components for the variance–covariance orientation test-setup.

Parallel analysis	#PC	% explained
LEFT	32	89.58
RIGHT	33	89.46
INTER	30	90.09
INTRA	39	86.79

the permutation-based version of the formal test for bilateral symmetry given by Mardia et al. (2000).

Firstly, the subspaces of the left and right ears as separate groups were compared. Second, we compared the subspaces of intra- vs. inter-subject variations. The results on comparing shape subspaces are given in Table A1 and Fig. A1. When considering left and right as separate groups, the difference in both group location and scale was significant. However, both differences show small effect-sizes: Cohen's distances of 0.08 and 0.18, respectively. Following Cohen's rule of thumb, these are lower than 'small' (0.2) and therefore the differences were considered trivial. This also implies that the effect of side or DA in overall ear shape can be considered trivial (Table A1). In combination with the non-significant difference in orientation, left and right subspaces covered the same loci in shape-space. When considering intra- and inter-subject shape variations (acquired from the AMMI framework) as separate groups, a non-significant effect was measured for group location. This is as it should be, simply because the intra-subject subspace was artificially centered on the overall average ear shape for visualization purposes only. A significant effect on group scale was observed with a Cohen's distance of 0.35, which is between a 'small' (0.2) and 'medium' (0.5) effect-size. This implies that the dispersion of inter-subject variations (5.23) was greater than the dispersion of intra-subject variations (4.75). In other words, differences between individuals are larger in magnitude than left–right differences, as was also seen in Fig. 3. Additionally and finally, besides group scale, a significant difference in orientation was observed as well, which implies that the patterns of inter- and intra-subject variations cover different directions in shape-space. This was observed primarily in the more pronounced changes occurring in the conchae, antitragus, and antihelix across individuals than with left–right patterns in Fig. 3.

The number of PCs used for testing group orientation differences was the maximum number of significant PCs for the respective subspaces compared pairwise (left/right and inter/intra) listed in Table A2 plus one. This to ensure that enough relevant variation was captured in the subspace representations without incorporating too much irrelevant variation. Two further observations are made from Table A2. Firstly, the number of PCs for left and right ear spaces separately were nearly equal, explaining a similar amount of total variance. Second, the number of significant PCs for intra-subject variations was larger than those of inter-subject variations, explaining the smaller amount of total variation. The larger the number of PCs required to explain a certain percentage of variance, the smaller the amount of redundancy or structure present within the data. Hence inter-subject variations were structurally more organized than intra-subject variations, which appear to be behaving more like noise. This is in line with the perception of fluctuating asymmetry resulting in the inability of a characteristic to develop in a pre-determined way (Van Valen, 1962).